Title

Programming alphavirus with IFN-γ overrides the adverse effects of macrophages on oncolytic virotherapy.

Authors

Laura Horvathova[1], Thijs Janzen[2], Baukje Nynke Hoogeboom[1], Franz J. Weissing[2], Toos Daemen[1], Darshak K. Bhatt[1]

1. Department of Medical Microbiology and Infection Prevention, University Medical Center Groningen, University of Groningen, Groningen, The Netherlands.
2. Groningen Institute for Evolutionary Life Sciences, University of Groningen, Groningen, The Netherlands

Abstract

Virus uptake by tumor-associated macrophages may significantly reduce the availability of oncolytic viruses for cancer cell infection and limit therapeutic efficacy. Through a computational model, we hypothesized that oncolytic viruses encoding a T cell-stimulating signal like IFN-γ can enhance efficacy regardless of macrophages. To test this, we engineered an alphavirus-based replicon expressing IFN-γ and studied its effect in various tumor-immune coculture systems. While alphavirus replicons do not replicate in macrophages, macrophages readily take up the virus, limiting tumor infection in a frequency-dependent but phenotype-independent manner. However, virus uptake activates the pro-inflammatory responses, further enhanced by neighboring cancer cells expressing virus-encoded IFN-γ. Consequently, T-cell activation was ensured even when a fraction of infected tumor cells expressed IFN-γ, regardless of macrophage presence, frequency, or phenotype. These findings suggest a strategy for optimizing oncolytic virotherapy in tumors with high macrophage infiltration by designing viruses that can stimulate T-cell activation, ensuring therapeutic efficacy.

Keywords

oncolytic RNA replicons, tumor-associated macrophages, therapeutic resistance, computational model, tumor-immune coculture

Introduction

Tumor-associated macrophages are a predominant component of the tumor immune infiltrate across many cancers[1]. These macrophages exhibit context-dependent phenotypic plasticity[2,3] and function to either support or suppress antitumor immunity[2–5]. In particular, they perform phagocytosis, act as antigen-presenting cells, express checkpoint regulators, and secrete an array of cytokines that shape cancer progression and response to immunotherapy[4,6,7].

Oncolytic virotherapy is a form of immunotherapy where viruses are used to infect and kill cancer cells, and subsequently boost tumor-specific immune responses[8]. Virus-induced cancer cell death causes the release of danger signals and antigens in the tumor microenvironment[9]. Ideally, these signals are immunogenic, enhancing the recruitment and proinflammatory activation of immune cells into the tumor. However, tumor-associated macrophages may hinder the therapeutic efficacy of oncolytic viruses by capturing virus particles, thereby significantly reducing the availability of the virus for infecting cancer cells[10–13]. This effect could be particularly pronounced when macrophages are non-permissive for viral replication, as it restricts the release of immunostimulatory signals and tumor antigens, thereby indirectly suppressing downstream immune activation. Tumor-associated macrophages further limit oncolysis through innate antiviral signaling[10–13] and T-cell suppression by regulatory mechanisms[3,14]. Variation in tumor composition[15,16], particularly in terms of macrophage frequency and phenotype can lead to variability in therapeutic responses[17–19]. Therefore, development of an oncolytic virotherapy that robustly stimulates T-cell immune responses is crucial to overcome the limitations posed by non-permissive macrophages.

Semliki Forest virus (SFV)-based replicons are emerging as promising candidates for immunogenic oncolytic virotherapy. SFV is a positive-stranded RNA virus, belonging to the *Alphavirus* genus. The RNA genome of SFV functions as a replicon, encoding non-structural viral proteins capable of viral-RNA translation and replication. Previous efforts in developing recombinant SFV particles (rSFV) have focused on improving safety by deleting viral genes that code for structural proteins[20]. This creates suicidal virus particles capable of a single round of infection. We and others have demonstrated that rSFV particles can successfully infect and express viral genes in a wide range of cancer cells and healthy stromal cells, however, macrophages are non-permissive to SFV infections and virus-encoded protein translation[21–23]. Furthermore, the immunogenicity of rSFV has been improved by encoding antigens[24–27], cytokines[22,28], or antibodies[29] to boost humoral and cellular immune responses in the context of cancer therapy and vaccination against infectious diseases. Our group has demonstrated phase-1 and phase 2 clinical safety, immunogenic potential and clinical efficacy of an rSFV-based therapeutic vaccine encoding antigens of human papillomavirus in patients with cervical cancer[30,31]. So far, studies using rSFV as an oncolytic agent have only been conducted in murine models[22,28,29]. Recently our group showed that rSFV can be engineered to express immunogenic human cytokines or chemokines with an enhanced potential to recruit and activate T-cells in different human cancer models[23].

In this study, we implemented a combined theoretical and experimental approach to design an immunogenic-rSFV therapy capable of T-cell activation regardless of the presence and activity of macrophages. As a proof-of-concept, we performed all the study analyses in the context of two independent solid tumor types, i.e. cervical and pancreatic cancer. First, we confirmed whether indeed macrophages limit rSFV infection in cancer cells growing in monolayer (2D, two-dimensional) or spheroid-based (3D, three-dimensional) tumor-macrophage cocultures. Second, we employed a computational model to assess whether rSFV-encoding immunogenic signals can promote anticancer T-cell responses and tumor eradication despite the presence of macrophages. Third, we surveyed the literature systematically to identify interferon-gamma (IFN-γ) as a pro-inflammatory cytokine capable

of both macrophage and T-cell activation. We further evaluated the correlation between intra-tumoral IFN-γ signature and activation of macrophages and T-cells using data of cervical and pancreatic cancer patients available from The Cancer Genome Atlas (TCGA)[1]. Finally for experimental validation, we engineered rSFV to express IFN-γ upon infection of cancer cells and employed both monolayer and spheroid-based tumor-immune cocultures to evaluate T-cell activation. In these tumor-immune cocultures, we introduced macrophages of either a naïve (M_{naive}) or an IL-4-induced phenotype (M_{IL4}). These models allowed us to assess how tumor infection and T-cell activation are influenced by macrophages and to evaluate the immunogenic potential of virus-encoded IFN-γ.

Results

Effect of macrophage frequency and phenotype on rSFV-mediated tumor infection

rSFV-mediated infection of cancer cells leads to expression of encoded transgenes but not production of progeny virus particles (as illustrated in **Figure 1A**). To validate our findings in an experimental setup, we employed an *in vitro* cancer-macrophage coculture model in either a monolayer or spheroid-based spatial organization (**Figure 1B**). This allowed us to have good control over factors such as the frequency and phenotype of macrophages and cancer cells. Using real-time microscopy-based imaging, we studied the effect of macrophages in regulating rSFV infection of a pancreatic cancer cell line (PANC-1). Figure 1C-D shows microscopy images resulting from the spheroid (**Figure 1C**) or monolayer (**Figure 1D**) coculture setup consisting of cancer cells and a varying frequency of macrophages. With an increasing frequency of macrophages (stained red in the images) present in the coculture, we observed a decrease in virus infection (stained green, expressing virus-encoded green fluorescent protein, GFP). We performed the cancer-macrophage coculture in various setups, either varying only the frequency of macrophages or the frequencies of both macrophages and cancer cells (**Figure 1E**). In particular, we confirmed[21,36] that virus-encoded GFP expression is restricted to cancer cells but not macrophages. The decrease in the number of infected cells corresponds to a decrease in the absolute number of target cancer cells and to a relative increase in the number of macrophages (**Figure 1F-G**).

As macrophages exhibit a wide range of phenotypes in the tumor microenvironment, we polarized them to either a classically activated anti-tumoral phenotype (M_{class} or M1-like) or an alternatively activated pro-tumoral phenotype (M_{alter} or M2-like) through cytokine stimulation (**Figure 2A**). Here, we used either a combination of LPS and IFN-γ to generate classically activated macrophages ($M_{LPS+IFNγ}$), or IL-4 to generate alternatively activated macrophages (M_{IL4}). Pro-inflammatory cell surface marker proteins such as CD80 and CD86 are upregulated in classically activated $M_{LPS+IFNγ}$ macrophages, whereas regulatory markers like CD206 are more abundant in alternatively activated M_{IL4} macrophages (**Figure 2B**) also corresponding to a distinct cellular state (**Figure 2C**). We then assessed if the macrophage phenotype, in particular the alternatively activated M_{IL4} phenotype that is most frequently found in tumors, influenced tumor infection by rSFV in monolayer or spheroid cocultures (**Figure 2D-E**). We observed that the number of GFP+ cells reduced with an increase in the number of macrophages, however, independent of the macrophage phenotype (**Figure 2F-G**). This was also the case when macrophages were cocultured with a cervical cancer cell line (Ca-Ski) (**Figure 2H**).

Model predictions regarding the effectiveness of immunogenic-rSFV therapy

In a previous study, we developed a spatiotemporal model to assess the effect of anticancer T-cell responses in response to immunogenic signals released upon oncolytic virotherapy[34,35]. **Figure 3A** (left image) depicts a snapshot of a computer simulation with a tumor containing uninfected cancer cells, virus-infected cancer cells, and macrophages. Upon infection-caused cell death, virus-induced

immunogenic signals are released in the neighborhood (as depicted in **Figure 3A** right and illustrated in **Figure 3B**) stimulating anticancer T-cell response. Using this model, we assessed the efficacy of rSFV encoding immunogenic signals as a non-replicating suicidal virotherapy. To estimate therapeutic success, we assessed the probability of tumor eradication caused by rSFV-infection and anticancer T-cell cytotoxicity. Panels **C** to **E** show - for five scenarios regarding the percentage of initially infected tumor cells - how the probability of tumor eradication is related to the IFN-γ level produced per infected cell (**Figure 3C**), the degree of T-cell cytotoxicity (**Figure 3D**), and the frequency of macrophages at the time of rSFV therapy (**Figure 3E**). Generally, 30% initially infected cells are sufficient to promote tumor eradication even at low levels of immunogenic signal production. A T-cell cytotoxicity level of 3 (corresponding to 3 target cells killed per cytotoxic T-cell per day) is required for an effective therapeutic outcome. Therapeutic outcome was found to be mainly determined by the percentage of initially infected cells producing immunogenic signals and not by the macrophage frequency.

The association between IFN-γ and macrophage-T-cell activation

We analyzed current literature to screen potential immunomodulatory cytokines produced and/or consumed by T-cells and macrophages. IFN-γ produced by T-cells was found to be a unique antitumoral cytokine that has the potential to stimulate both macrophages and T-cells through JAK-STAT signaling pathway (**Figure 4A**) with an effective concentration ranging from 3 to 40 pM (**Figure 4B**)[32].

Based on cervical and pancreatic cancer patient data from TCGA[1,33], we analyzed the correlation between the IFN-γ signature in tumor samples with the frequency of macrophages and T-cells and the phenotype of macrophages (**Figure 4C**). **Figure 4D** shows an overview of the correlation between the intra-tumoral IFN-γ signature and different phenotypes of macrophages and cytotoxic CD8 T-cells. The IFN-γ signature was found to positively correlate with a classically activated (M_{class} or M1-like) pro-inflammatory macrophage phenotype in both cervical (CESC) and pancreatic (PAAD) tumor samples (**Figure 4E, 4G**) but not with an alternatively activated (M_{alter} or M2-like) immunosuppressive macrophage phenotype (**Figure 4F, 4H**). As T-cells are one of the primary cells producing IFN-γ, we analyzed if there was a correlation between intra-tumoral CD8 T-cells and a particular macrophage phenotype (**Figure 4I**). We observed a positive correlation between classically activated (M_{class}) proinflammatory macrophages and the frequency of intra-tumoral CD8 T-cells (**Figure 4J, 4L**). Inversely, there was a negative correlation between alternatively activated (M_{alter}) immunosuppressive macrophages and CD8 T-cell frequency (**Figure 4K, 4M**).

T cell activation by rSFV in the presence of macrophages

We treated tumor-immune monolayer cocultures of macrophages and cancer cells with rSFV and added peripheral blood mononuclear cells (PBMCs) to the culture to introduce T-cells and evaluate their activation (**Figure 5A**). Through flow cytometry, we quantified cell-surface expression of immune activation (CD69, CD38) and cytotoxic-degranulation (CD107a) markers as a proxy of CD4 (helper) and CD8 (cytotoxic) T-cell activation. T-cells were considered fully activated when simultaneously positive for CD38, CD69, and CD107a expression. **Figure 5B and 5C** illustrate the population distribution of activated CD4 and CD8 T-cells in different scenarios of rSFV infection and tumor-immune cocultures consisting of either PANC-1 cells or Ca-Ski cells in culture with M_{naive} or M_{IL4} macrophages in different frequencies. The upper right quadrant in each flow cytometry panel indicates the population of fully activated T-cells as characterized by the expression of CD69, CD107a and CD38.

We observed a decrease in CD4 but not CD8 T-cell activation as a result of coculturing PBMCs solely with either M_{naive} or M_{IL4} macrophages (black circle/line, **Figure 5D**, 6E leftmost panel). PBMC coculture with cancer cells alone or in the presence of increasing frequency of either M_{naive} or M_{IL4} macrophages also led to a similar decrease in CD4 T-cell activation when compared to PBMCs alone (black circle/line, **Figure 5D**). rSFV particles themselves in the absence of target cancer cells did not have any immunomodulatory effects on CD4 or CD8 T-cell activation directly (green circle/line, **Figure 5D, 5E**, leftmost panel). Upon rSFV-GFP therapy, i.e. not encoding IFN-γ, CD8 T-cell activation was only observed in the case of infecting Ca-Ski cells but not PANC-1 cells and was independent of macrophage presence or phenotype (green circle/line, **Figure 5E**, rightmost panel). Upon rSFV-IFN-γ (rSFV-encoding IFN-γ) treatment, however, both CD4 and CD8 T-cells were activated independently of infecting Ca-Ski cells or PANC-1 cells (red circle/line, **Figure 5D, 5E**). Here, CD4 T-cell activation increased with an increasing number of either M_{naive} or M_{IL4} macrophages present in the coculture (**Figure 5D**).

Next, we assessed T-cell activation in spheroid-based tumor-immune cocultures (**Figure 6A**). In contrast to the results from the monolayer-based coculture system, we observed a decrease in the number of activated CD4 T-cells with an increasing frequency of macrophages in the coculture (black circle/line, **Figure 6B**). However, similar to the results from the monolayer coculture, we observed that rSFV-GFP particles only induced CD8 T-cell activation in the case of infecting Ca-Ski cells but not PANC-1 cells (green circle/line, **Figure 6C**, rightmost panels). Moreover, rSFV-IFN-γ also led to a higher frequency of activated CD4 and CD8 T-cells independent of infecting Ca-Ski cells or PANC-1 cells (red circle/line, **Figure 6B, 6C**). Here, CD4 and CD8 T-cell activation even improved further with an increasing frequency of either M_{naive} or M_{IL4} macrophages.

Multimodal activation of macrophages by rSFV-IFN-γ

Recently our group has shown that rSFV replicon virus particles have a direct influence on macrophage phenotype and can lead to their pro-inflammatory activation independent of their initial state[36]. Consequently, we evaluated if macrophages are also stimulated by infected cancer cells alone and if there is any additional effect in combination with virus-mediated activation (**Figure 7A**). To quantify this response, we assessed the change in expression of costimulatory molecules (CD80, CD86) on macrophages involved in T-cell regulation in addition to CD206 expression that is often associated with a regulatory phenotype and poor cancer prognosis. IL-4 polarized (M_{IL4}) regulatory macrophages were found to upregulate CD86 and CD80 cell-surface expression upon stimulation with either only rSFV particles (**Figure 7B**) or only PANC-1 infected cells expressing virus-encoded IFN-γ (**Figure 7C**) or both (**Figure 7D**). The upregulation of CD80 and CD86 was the highest when

macrophages received simultaneous stimulation by virus particles and infected cells producing virus-encoded IFN-γ. Importantly, significant downregulation of cell-surface CD206 expression was observed when macrophages were stimulated with infected cells producing virus-encoded IFN-γ but not GFP.

We further confirmed that both naïve (M_{naive}) and regulatory (M_{IL4}) macrophages upregulate CD80 and CD86 cell-surface expression upon stimulation with rSFV replicon particles (**Figure 7F**). Moreover, CD206 downregulation and a strong CD80 and CD86 upregulation were observed when either of the macrophage types was stimulated simultaneously with rSFV particles and infected cancer cells expressing virus-encoded IFN-γ (**Figure 7G-J**). This observation holds true for both PANC-1 (panel **G-H**) and Ca-Ski (**panel I-J**) cancer cell lines.

Discussion

In this study, we investigated how macrophages impact the therapeutic efficacy of rSFV-based oncolytic therapy. Our findings validate that macrophages, irrespective of their phenotype, take up rSFV replicon particles but do not translate rSFV-encoded proteins[37]. Thereby macrophages can impede virus infection of tumor cells. This highlights a significant barrier to effective oncolytic virotherapy, as the presence of macrophages can limit the infection and subsequent oncolytic activity of the virus, potentially reducing the overall therapeutic outcome[17,34]. Leveraging a computational modelling approach, we hypothesized that arming oncolytic viruses to express immunogenic signals like IFN-γ could stimulate robust T-cell activation and enhance tumor eradication despite the presence of macrophages. This was experimentally validated in both monolayer and spheroid-based tumor-immune cocultures. Overall, our results demonstrate the potential of a combined theoretical and experimental approach in improving the immunogenic potential of oncolytic virotherapy despite the presence of macrophages.

Our computational modeling results provided insights into the spatiotemporal dynamics of rSFV-IFN-γ therapy and its potential despite an abundant presence of macrophages. Our model demonstrated that the release of IFN-γ at effective concentrations is vital for achieving robust T-cell activation and subsequent tumor eradication. Specifically, the model underscored the importance of achieving the effective concentration threshold via either increasing the number of infected cells in the tumor or by improving IFN-γ production by individual infected cells; in both cases ensuring activation of anticancer cytotoxic T-cells to mount a strong antitumor response. The model also highlighted the importance of T-cell cytotoxicity in the success of rSFV-IFN-γ therapy. A minimally required cytotoxicity rate of three target cells killed per day by each cytotoxic T-cell, comparable to what is noted in the literature[38], was found to be essential for effective tumor eradication. This emphasizes that alongside the production of IFN-γ, the intrinsic killing efficiency of T-cells is a critical factor in the overall therapeutic outcome. Importantly, the model predicted that the therapeutic success is largely independent of the number of macrophages present at the time of treatment. This suggests that rSFV-IFN-γ can effectively overcome the influence of macrophages non-permissive for SFV, provided that the thresholds for infected cells and T-cell cytotoxicity are met. These findings collectively underscore the potential of rSFV-IFN-γ oncolytic virotherapy to enhance antitumor responses by leveraging the synergistic effects of targeted viral infection and potent immune activation, regardless of the presence of macrophages.

Based on our empirical findings, we confirm that rSFV while not productively infecting macrophages leads to their immunogenic activation. Importantly, as the frequency of macrophages in coculture with cancer cells increased, the infectivity of the cancer cells decreased in both monolayer and spheroid-based settings. We confirmed that macrophages themselves did not allow rSFV-encoded

transgene expression, which can likely be attributed to innately active antiviral signaling pathways. This is in line with our previous work[36] and the observations made by Olupe Kurena and colleagues[37]. Multiple oncolytic viruses have been shown to activate macrophages during therapy, both through direct virus-uptake and signaling from infected cancer cells[39–43]. Specifically for replication-competent oncolytic viruses, macrophage activation has also been attributed to therapeutic resistance due to virus-uptake by macrophages, antiviral signaling (e.g. via TNF-α or IFN pathway) and killing of infected cancer cells to inhibit virus replication[42–44]. In case of replication-deficient oncolytic viruses like rSFV, previous studies have demonstrated that sensing of viral RNA by various endosomal toll-like receptors (TLRs) and cytosolic retinoic acid-inducible gene I (RIG-I) receptor can result in degradation of viral RNA to downregulate viral-protein expression in macrophages[9]. However, TLR and RIG-I mediated sensing also may lead to the proinflammatory activation of macrophages[45,46]. In line with our previous study[36], we observed that macrophages upregulate CD80 and CD86 surface protein expression upon virus-uptake, corresponding to a stronger co-stimulatory signaling for antigen presentation. A similar macrophage activation profile was observed independent of their initial naïve (M_{naive}) or regulatory (M_{IL4}) macrophage phenotype. Various groups have demonstrated so far that although macrophages demonstrate functionally distinct phenotypes[47,48], they are capable of switching through these phenotypes in response to environmental stimuli within 48 hours[49,50]. Despite their adaptability, macrophages maintain their non-permissive nature towards rSFV-mediated transgene expression independent of their initial phenotype and their switch towards a pro-inflammatory phenotype upon rSFV-uptake.

Engineering rSFV to encode IFN-γ enhanced macrophage polarization to a proinflammatory phenotype. Macrophages upregulated pro-inflammatory markers (CD80, CD86) and downregulated pro-tumoral markers (CD206) to a significantly higher magnitude when in the presence of infected cancer cells expressing rSFV-encoded IFN-γ, as compared to being stimulated by virus alone or SFV-GFP infected cancer cells. We assume this to be a result of the bimodal stimulation by virus-uptake and extracellular sensing of IFN-γ. Previous studies have demonstrated that either type-I or type-II IFNs are required for macrophages to polarize towards a strongly pro-inflammatory phenotype when stimulated by stress signals like extracellular release of heat-shock proteins or danger signal like bacterial lipopolysaccharides and viral RNA[48,49,51]. Therefore, it is likely that the intracellular release of rSFV-RNA upon virus uptake in the macrophages and extracellular IFN-γ produced by neighboring infected cancer cells results in their proinflammatory activation. As we did not observe rSFV-mediated transgene expression by macrophages, we consider that rSFV-encoded IFN-γ expression is limited to infected cancer cells and that IFN-γ is not sensed in an autocrine manner by macrophages.

Our study demonstrates that rSFV-encoding IFN-γ significantly stimulates T-cell responses, independent of the influence of macrophages. This was observed across both monolayer (2D) and spheroid (3D) cocultures, highlighting the robustness of this approach. In monolayer cocultures, the presence of rSFV-IFN-γ led to pronounced activation of both CD4 and CD8 T-cells, even in the presence of high macrophage frequencies. Notably, macrophages, despite their non-permissiveness to SFV infection and potential for antiviral signaling, did not impede T-cell activation induced by rSFV-IFN-γ. This finding underscores the potential of IFN-γ as a powerful immunostimulatory cytokine that can override the suppressive effects of macrophages in the tumor microenvironment. Furthermore, the impact of macrophage phenotype and frequency on T-cell responses varied between monolayer and spheroid cocultures. In monolayer systems, macrophages reduced CD4 but not CD8 T-cell activation, suggesting a differential regulatory effect on helper versus cytotoxic T-cells. However, in spheroid cocultures, an increase in macrophage frequency led to a reduction in activation of both CD4 and CD8 T-cells. Despite these variations, rSFV-IFN-γ consistently promoted strong T-cell responses regardless of either a naïve (M_{naive}) or regulatory (M_{IL4}) macrophage phenotype. Finally, in

both monolayer and spheroid cocultures, a high frequency of macrophages correlated to a stronger CD4 T-cell activation by rSFV-IFN-γ, which may be attributed to rSFV-mediated proinflammatory activation of the macrophages. Observations of Meissner et al. corroborate our results, that encoding IFN-γ by a non-replicating oncolytic virus, influenza A virus in their case, can promote tumor eradication through enhanced immune responses and not primarily through virus-mediated oncolysis[52]. Indeed, a replication-competent oncolytic virus causing extensive virus-mediated oncolysis in combination with IFN-γ mediated immune stimulation can also lead to tumor eradication albeit with a risk of virus persistence[53].

In conclusion, our study presents a compelling case for the use of rSFV-encoding IFN-γ as a means to enhance antitumor immune responses, effectively overcoming macrophage-mediated regulation of virus-infection and T-cell activation. The combination of computational modeling with experimental validation in diverse human tumor models, provides evidence supporting this therapeutic strategy. Future studies should explore the clinical translation of these findings, assessing the efficacy of rSFV-IFN-γ in preclinical models like patient-derived organoids to test its therapeutic potential in a patient-specific manner. The significant implications of our findings lie in their potential to inform the design of oncolytic virotherapies, especially for tumors characterized by high macrophage infiltration and immune suppression.

Limitations of the study: While our study demonstrates the potential of rSFV-encoding IFN-γ in enhancing T-cell immune responses, several limitations must be acknowledged. One significant limitation is the lack of direct measurement of T-cell-mediated antitumor killing. Although we showed robust T-cell activation, the subsequent cytotoxic activity of these T-cells against tumor cells was not quantified due to the unavailability of a tumor-specific T-cell model for our experiments. Furthermore, our study does not fully account for the complex interactions within the tumor immune microenvironment, focusing primarily on T-cell responses. This narrow focus may overlook the broader spectrum of immune cell dynamics and the potential contributions of other immune cells, such as natural killer cells and dendritic cells. Additionally, the in vitro coculture models, while informative, do not fully replicate the *in vivo* tumor microenvironment. Expanding the study to include patient-derived organoids and diverse tumor types will be essential to validate these findings and to fully understand the therapeutic potential of rSFV-encoding IFN-γ in a clinical setting.

Materials and methods

TCGA analysis: We used the online CRI iAtlas portal to analyze TCGA data of cervical and pancreatic cancer patients[1,33]. We selected the TCGA cohort of cervical cancer (CESC) patients (n=300) and pancreatic cancer (PAAD) patients (n=151). Performed Pearson correlation to analyze the relationship between IFN-γ signature, cytotoxic CD8 T-cells, and pro-tumoral (M2-like or M_{alter}) or anti-tumoral (M1-like or M_{class}) macrophages. IFN-γ signature and immune cell subset quantifications of the tumor samples were performed previously as a part of the immune landscape analysis of cancer[1,33].

Computational model: In our previous work[34,35], we developed a spatiotemporal model for the effect of oncolytic virotherapy on tumor development to evaluate how anticancer T-cell responses triggered by immunogenic signals affect the therapeutic outcome. In the current study, we employed the model to simulate a tumor environment with three cell types: stromal macrophages, uninfected infection-sensitive cancer cells, and infected cancer cells. We assumed that infection-sensitive cancer cells and stromal macrophages are initially distributed randomly. Cells can divide, change status, or die, with varying rates across cell types. Cancer cells can be infected by an oncolytic virus, which targets and kills them, while stromal macrophages are non-permissive to infection. Since rSFV is a non-replicating virotherapy, no further viral spread occurs in the model. We incorporated a cell-specific immune response to assess how virus-induced immunogenic signals influence therapeutic outcomes. The model assumes that infection-induced cell death induces the release of immunogenic signals, which diffuses and subsequently activates T-cells to kill cancer cells, with cytotoxicity of the activated T-cells depending on the local concentration of immunogenic signals. Key variables assessed in this study include the percentage of infected cancer cells, amount of immunogenic signal released per infected cell, T-cell cytotoxicity rate, and macrophage frequency. Immunogenic molecules are initially absent and increase in concentration (λ) in the grid cell upon infection-induced cell death. Immunogenic signals disperse to neighboring cells via diffusion and diminishes over time due to evaporation. In our previous studies, the model revealed that therapeutic outcomes are probabilistic. To account for this, we ran 10,000 simulations per parameter combination to capture stochastic variations in the results. Since rSFV is a suicidal virotherapy and does not replicate, the model predicted two possible outcomes at 1,000 days: (i) total tumor eradication, where all cancer cells are eliminated; or (ii) tumor persistence, where cancer cells survive due to insufficient virus- and/or immune-mediated killing. For this study, we focused on the probability of total tumor eradication as the primary outcome. A detailed description of the model can be found in references 33 and 34. The code used for this work and an executable version of the Oncolytic Virus Immune simulator (OVI) can be found at www.github.com/rugtres/OVI/tree/init_random.

Cell culture: BHK-21, Ca-Ski, and Panc-1 cells were cultured in RPMI 1640 medium supplemented with 10% fetal bovine serum (FBS), 100 U/ml penicillin, and 100 µg/ml streptomycin (P/S, Thermo Scientific). Since, PANC-1 and Ca-Ski cells are HLA-2A-restricted, we performed the cancer-immune coculture assays with peripheral blood mononuclear cells (PBMCs) derived from HLA-2A-matched healthy donors (Sanquin, Netherlands). Cancer cell-macrophage cocultures were cultured in RPMI 1640 medium supplemented with 10% FBS and 100 U/ml penicillin, 100 µg/ml streptomycin. Cocultures with PBMCs were similarly cultured in RPMI 1640 medium supplemented with 10% FBS and 100 U/ml penicillin, 100 µg/ml streptomycin. For spheroid cocultures, cells were seeded in NuncSphera round-bottom 96-well plates (Thermo Fischer) and centrifuged for 10 minutes at 1500 RPM. All cells were maintained in an incubator at 37°C with 5% CO_2.

Monocyte derived macrophage differentiation and polarization: Peripheral blood derived monocytes were differentiated to macrophages and polarized in RPMI 1640 medium supplemented with 10%

FBS, 100 U/ml penicillin, 100 µg/ml streptomycin, 1mM sodium pyruvate (Thermo Scientific), non-essential amino-acids (NEAA, Thermo Fisher), and 100 ng/mL macrophage colony-stimulating factor (M-CSF, BioLegend San Diego, CA, USA). Briefly, PBMCs from healthy donors were cultured for 2 hours to allow monocyte adherence. Afterward, non-adherent cells were gently removed. The adhered cells were stimulated with M-CSF. The medium containing M-CSF was refreshed on 3 days post culture. Macrophages were replated on 7 days of culture. 24 hours later, macrophages were polarized to either a M_{IL4} state with medium containing 20 ng/mL IL-4 (BioLegend, San Diego, CA, USA), or a M1-like state with medium containing 20 ng/ml IFN-γ and 100 ng/ml lipopolysaccharides, or were kept unstimulated (M_{naive}).

Design, production and titer determination of rSFV: We have previously designed rSFV-replicon particles expressing immunogenic transgenes and capable of a single round of infection[23,54]. Briefly, enhanced green fluorescent protein (GFP) and IFN-γ as transgenes were ordered as a DNA construct (Eurofins Genomics, Ebensburg, Germany) and were cloned in the SFV-replicon backbone plasmid (pSFV) by using PspOMI and XmaI as restriction sites and *E. coli* JM110 as the competent cell chassis. Sanger sequencing was performed on isolated clones to validate insertion (Eurofins Genomics). pSFV containing either GFP or IFN-γ and a SFV-Helper-2 plasmid (hSFV) were linearized with SpeI digestion (Life Technologies) for in vitro RNA synthesis by SP6 polymerase reaction (Amersham Pharmacia Biotech, Piscataway, US). Next, pSFV-transgene RNA and hSFV RNA were mixed in a 2:1 ratio and co-transfected in BHK21 cells in the presence of electroporation buffer using the BioRad Gene Pulser II system (2 pulses, 850 V/25 µF; Biorad, Hercules, U.S.A.). After electroporation, the cells were cultured in RPMI 1640 media supplemented with 5% FBS, 100 U/ml penicillin, and 100 µg/ml streptomycin for 48 hours at 30°C with 5% CO_2. The rSFV-transgene particles were purified by discontinuous sucrose density gradient ultracentrifugation and stored in TNE buffer as aliquots at -80°C. Before use, all rSFV particles were activated by the addition of 1:20 volume 10 mg/ml α-chymotrypsin (Sigma Chemical, St. Louis, US) and 2 mM $CaCl_2$ for 30 minutes to cleave the mutated spike proteins. After which, the α-chymotrypsin was inactivated by the addition of 1:2 volume 2 mg/ml aprotinin (Sigma Chemical). Finally, the titer determination of rSFV-particles was performed as described previously. Briefly, rSFV-particles were titrated by serial dilution on monolayers of BHK-21 cells cultured in LabTek slides. After infection and incubation for 24 hours, the cells were fixed in 10% (w/v) acetone and further stained for nsP3 using a primary polyclonal rabbit-anti-nsP3 antibody (1:2000 dilution), whilst a secondary Cy3-labeled animal-anti-rabbit antibody (1:200 dilution) was used to amplify the signal. Positive cells were counted using fluorescence microscopy, and the titers were determined.

Evaluating virus-infection in macrophage-cancer cell cocultures: M_{naive} or M_{IL4} macrophages were differentiated from human PBMCs as described above. Different frequencies of M0 or M_{IL4} macrophages were cocultured with either a constant or variable frequency of Panc-1 or Ca-Ski cancer cells. After overnight incubation, cocultures were infected with an MOI of 10 (multiplicity-of-infection) of rSFV-GFP. The ability of rSFV-particles to infect cells and express GFP was monitored over 24 hours by Incucyte-based brightfield and fluorescence microscopy. The number of GFP-positive cells served as a measure of the rSFV-GFP particle's infectivity.

Evaluating macrophage activation by virus particles and infected cancer cells: M_{naive} or M_{IL4} macrophages were differentiated from human PBMCs as described above. M0 or M_{IL4} macrophages were cocultured in a 1:2 ratio with Panc-1 or Ca-Ski cells in a 24-well plate. After overnight incubation, cocultures were infected with MOI-10 of rSFV-GFP or rSFV-IFNγ. 24 hours post-infection (HPI), all cells were collected and processed for Flow cytometry-based analysis of macrophage activation markers.

Evaluating T-cell activation in tumor-immune cocultures: M_{naive} or M_{IL4} macrophages were differentiated as described above, from HLA-2 typed healthy donors. They were cocultured with Panc-1 cells or Ca-Ski cells for 24 hours in 2 tumor cells to 1 macrophage cell ratio (15 000 cells per well) in a treated 96-well plate. Cocultures were then infected with MOI-10 of rSFV-particles encoding GFP or IFN-γ. 8 hours post-infection, freshly thawed PBMCs from the same donor were added to the cocultures (75 000 cells per well). 18 hours post PBMCs addition, all cells were collected and stained for CD4 and CD8 T-cell population, as well as immune activation cell surface markers, and analyzed *via* Flow cytometry. The gating strategy is illustrated in **Supplementary Figure 1**.

Quantification and statistical analysis: Experimental data represents the mean ± SEM of the number of replicates. Graphs were made using Rstudio, RawGraphs, and Graphpad Prism 10.

Table 1 Anti-human antibodies used in Flow cytometry.

Antibody target	Producer	Catalog#
FITC anti-human CD4 OKT4	Biolegend	317408
APC/Cyanine-7 anti-human CD8 SK11	Biolegend	344714
Brilliant violet 421TM anti-human CD38 HIT2	Biolegend	303526
APC anti-human CD69 FN50	Biolegend	310910
PE anti-human CD107a H4A3	Biolegend	328608
PE anti-human CD11b ICRF44	Biolegend	301306
APC-Fire anti-human CD206 15-2	Biolegend	321133
APC anti-human CD80 2D10	Biolegend	374204
FITC anti-human CD86 BU63	Biolegend	328608
PE anti-human CD163 Antibody	Biolegend	333605
PE/Cyanine7 anti-human CD68 Antibody	Biolegend	333815
APC anti-human CD206 (MMR) Antibody	Biolegend	321109
Brilliant Violet 421™ anti-human CD80 Antibody	Biolegend	305221

Acknowledgements
Part of the work has been performed at the UMCG Imaging and Microscopy Center (UMIC) and the Flow Cytometry Research Unit (FCU) which is sponsored by UMCG.

Author contributions
DB: Conceptualization, Writing and editing manuscript, Data collection and analysis, Software, Visualization, Supervision
LH: Writing and editing manuscript, Data collection and analysis, Validation, Visualization
TJ: Conceptualization, Writing and editing manuscript, Software, Data analysis, Visualization, Supervision
BNH: Writing and editing manuscript, Data collection and analysis, Validation, Visualization
FJW: Conceptualization, Writing and editing manuscript, Supervision
TD: Conceptualization, Writing and editing manuscript, Supervision, Funding acquisition

Declaration of interests
The authors declare no competing interests.

References

1. Thorsson, V., Gibbs, D.L., Brown, S.D., Wolf, D., Bortone, D.S., Ou Yang, T.-H., Porta-Pardo, E., Gao, G.F., Plaisier, C.L., Eddy, J.A., et al. (2018). The Immune Landscape of Cancer. Immunity *48*, 812-830.e14. https://doi.org/10.1016/j.immuni.2018.03.023.

2. Park, M.D., Silvin, A., Ginhoux, F., and Merad, M. (2022). Macrophages in health and disease. Cell *185*, 4259–4279. https://doi.org/10.1016/j.cell.2022.10.007.

3. Biswas, S.K., and Mantovani, A. (2010). Macrophage plasticity and interaction with lymphocyte subsets: cancer as a paradigm. Nat Immunol *11*, 889–896. https://doi.org/10.1038/ni.1937.

4. Fridman, W.H., Zitvogel, L., Sautès–Fridman, C., and Kroemer, G. (2017). The immune contexture in cancer prognosis and treatment. Nat Rev Clin Oncol *14*, 717–734. https://doi.org/10.1038/nrclinonc.2017.101.

5. Cassetta, L., and Pollard, J.W. (2023). A timeline of tumour-associated macrophage biology. Nat Rev Cancer *23*, 238–257. https://doi.org/10.1038/s41568-022-00547-1.

6. Gooden, M.J.M., de Bock, G.H., Leffers, N., Daemen, T., and Nijman, H.W. (2011). The prognostic influence of tumour-infiltrating lymphocytes in cancer: a systematic review with meta-analysis. Br J Cancer *105*, 93–103. https://doi.org/10.1038/bjc.2011.189.

7. Brummel, K., Eerkens, A.L., De Bruyn, M., and Nijman, H.W. (2023). Tumour-infiltrating lymphocytes: from prognosis to treatment selection. Br J Cancer *128*, 451–458. https://doi.org/10.1038/s41416-022-02119-4.

8. Russell, S.J., Peng, K.-W., and Bell, J.C. (2012). Oncolytic virotherapy. Nat Biotechnol *30*, 658–670. https://doi.org/10.1038/nbt.2287.

9. Bhatt, D.K., and Daemen, T. (2024). Molecular Circuits of Immune Sensing and Response to Oncolytic Virotherapy. IJMS *25*, 4691. https://doi.org/10.3390/ijms25094691.

10. Denton, N., Chen, C.-Y., Scott, T., and Cripe, T. (2016). Tumor-Associated Macrophages in Oncolytic Virotherapy: Friend or Foe? Biomedicines *4*, 13. https://doi.org/10.3390/biomedicines4030013.

11. Jakeman, P.G., Hills, T.E., Fisher, K.D., and Seymour, L.W. (2015). Macrophages and their interactions with oncolytic viruses. Current Opinion in Pharmacology *24*, 23–29. https://doi.org/10.1016/j.coph.2015.06.007.

12. Mealiea, D., and McCart, J.A. (2022). Cutting both ways: the innate immune response to oncolytic virotherapy. Cancer Gene Ther *29*, 629–646. https://doi.org/10.1038/s41417-021-00351-3.

13. Hofman, L., Lawler, S.E., and Lamfers, M.L.M. (2021). The Multifaceted Role of Macrophages in Oncolytic Virotherapy. Viruses *13*, 1570. https://doi.org/10.3390/v13081570.

14. DeNardo, D.G., and Ruffell, B. (2019). Macrophages as regulators of tumour immunity and immunotherapy. Nat Rev Immunol *19*, 369–382. https://doi.org/10.1038/s41577-019-0127-6.

15. Bhatt, D.K., Wekema, L., Carvalho Barros, L.R., Chammas, R., and Daemen, T. (2021). A systematic analysis on the clinical safety and efficacy of onco-virotherapy. Molecular Therapy - Oncolytics *23*, 239–253. https://doi.org/10.1016/j.omto.2021.09.008.

16. Li, Z., Jiang, Z., Zhang, Y., Huang, X., and Liu, Q. (2020). Efficacy and Safety of Oncolytic Viruses in Randomized Controlled Trials: A Systematic Review and Meta-Analysis. Cancers (Basel) *12*. https://doi.org/10.3390/cancers12061416.

17. Bhatt, D.K., Chammas, R., and Daemen, T. (2021). Resistance Mechanisms Influencing Oncolytic Virotherapy, a Systematic Analysis. Vaccines *9*, 1166. https://doi.org/10.3390/vaccines9101166.

18. de Gruijl, T.D., Janssen, A.B., and van Beusechem, V.W. (2015). Arming oncolytic viruses to leverage antitumor immunity. Expert Opin Biol Ther *15*, 959–971. https://doi.org/10.1517/14712598.2015.1044433.

19. Kaufman, H.L., Kohlhapp, F.J., and Zloza, A. (2015). Oncolytic viruses: a new class of immunotherapy drugs. Nature Reviews Drug Discovery *14*, 642–662. https://doi.org/10.1038/nrd4663.

20. Smerdou, C., and Liljeström, P. (1999). Two-helper RNA system for production of recombinant Semliki forest virus particles. J Virol *73*, 1092–1098. https://doi.org/10.1128/JVI.73.2.1092-1098.1999.

21. Kurena, B., Müller, E., Christopoulos, P.F., Johnsen, I.B., Stankovic, B., Øynebråten, I., Corthay, A., and Zajakina, A. (2017). Generation and Functional In Vitro Analysis of Semliki Forest Virus Vectors Encoding TNF-α and IFN-γ. Front. Immunol. *8*, 1667. https://doi.org/10.3389/fimmu.2017.01667.

22. Sánchez-Paulete, A.R., Teijeira, Á., Quetglas, J.I., Rodríguez-Ruiz, M.E., Sánchez-Arráez, Á., Labiano, S., Etxeberria, I., Azpilikueta, A., Bolaños, E., Ballesteros-Briones, M.C., et al. (2018). Intratumoral Immunotherapy with XCL1 and sFlt3L Encoded in Recombinant Semliki Forest Virus-Derived Vectors Fosters Dendritic Cell-Mediated T-cell Cross-Priming. Cancer Res. *78*, 6643–6654. https://doi.org/10.1158/0008-5472.CAN-18-0933.

23. Bhatt, D.K., Meuleman, S.L., Hoogeboom, B.N., and Daemen, T. (2024). Oncolytic alphavirus replicons mediated recruitment and activation of T-cells. iScience *27*, 109253. https://doi.org/10.1016/j.isci.2024.109253.

24. Draghiciu, O., Boerma, A., Hoogeboom, B.N., Nijman, H.W., and Daemen, T. (2015). A rationally designed combined treatment with an alphavirus-based cancer vaccine, sunitinib and low-dose tumor irradiation completely blocks tumor development. Oncoimmunology *4*, e1029699. https://doi.org/10.1080/2162402X.2015.1029699.

25. Ip, P.P., Boerma, A., Regts, J., Meijerhof, T., Wilschut, J., Nijman, H.W., and Daemen, T. (2014). Alphavirus-based vaccines encoding nonstructural proteins of hepatitis C virus induce robust and protective T-cell responses. Mol Ther *22*, 881–890. https://doi.org/10.1038/mt.2013.287.

26. Knudsen, M.L., Ljungberg, K., Tatoud, R., Weber, J., Esteban, M., and Liljeström, P. (2015). Alphavirus replicon DNA expressing HIV antigens is an excellent prime for boosting with recombinant modified vaccinia Ankara (MVA) or with HIV gp140 protein antigen. PLoS ONE *10*, e0117042. https://doi.org/10.1371/journal.pone.0117042.

27. Öhlund, P., García-Arriaza, J., Zusinaite, E., Szurgot, I., Männik, A., Kraus, A., Ustav, M., Merits, A., Esteban, M., Liljeström, P., et al. (2018). DNA-launched RNA replicon vaccines induce potent anti-Ebolavirus immune responses that can be further improved by a recombinant MVA boost. Sci Rep *8*, 12459. https://doi.org/10.1038/s41598-018-31003-6.

28. Quetglas, J.I., Labiano, S., Aznar, M.Á., Bolaños, E., Azpilikueta, A., Rodriguez, I., Casales, E., Sánchez-Paulete, A.R., Segura, V., Smerdou, C., et al. (2015). Virotherapy with a Semliki Forest Virus–Based Vector Encoding IL12 Synergizes with PD-1/PD-L1 Blockade. Cancer Immunology Research *3*, 449–454. https://doi.org/10.1158/2326-6066.CIR-14-0216.

29. Ballesteros-Briones, M.C., Martisova, E., Casales, E., Silva-Pilipich, N., Buñuales, M., Galindo, J., Mancheño, U., Gorraiz, M., Lasarte, J.J., Kochan, G., et al. (2019). Short-Term Local Expression of a PD-L1 Blocking Antibody from a Self-Replicating RNA Vector Induces Potent Antitumor Responses. Mol Ther *27*, 1892–1905. https://doi.org/10.1016/j.ymthe.2019.09.016.

30. Komdeur, F.L., Singh, A., van de Wall, S., Meulenberg, J.J.M., Boerma, A., Hoogeboom, B.N., Paijens, S.T., Oyarce, C., de Bruyn, M., Schuuring, E., et al. (2021). First-in-Human Phase I Clinical Trial of an SFV-Based RNA Replicon Cancer Vaccine against HPV-Induced Cancers. Mol Ther *29*, 611–625. https://doi.org/10.1016/j.ymthe.2020.11.002.

31. Eerkens, A.L., Esajas, M.D., Brummel, K., Vledder, A., Van Rooij, N., Plat, A., Avalos Haro, S.B., Paijens, S.T., Slagter-Menkema, L., Schuuring, E., et al. (2025). Vvax001, a Therapeutic Vaccine for Patients with HPV16-positive High-grade Cervical Intraepithelial Neoplasia: a Phase II Trial. Clinical Cancer Research. https://doi.org/10.1158/1078-0432.CCR-24-1662.

32. Altan-Bonnet, G., and Mukherjee, R. (2019). Cytokine-mediated communication: a quantitative appraisal of immune complexity. Nat Rev Immunol *19*, 205–217. https://doi.org/10.1038/s41577-019-0131-x.

33. Eddy, J.A., Thorsson, V., Lamb, A.E., Gibbs, D.L., Heimann, C., Yu, J.X., Chung, V., Chae, Y., Dang, K., Vincent, B.G., et al. (2020). CRI iAtlas: an interactive portal for immuno-oncology research. F1000Res *9*, 1028. https://doi.org/10.12688/f1000research.25141.1.

34. Bhatt, D.K., Janzen, T., Daemen, T., and Weissing, F.J. (2022). Modelling the spatial dynamics of oncolytic virotherapy in the presence of virus-resistant tumour cells. PLoS Comput Biol *18*, e1010076. https://doi.org/10.1371/journal.pcbi.1010076.

35. Bhatt, D.K., Janzen, T., Daemen, T., and Weissing, F.J. (2024). Effects of virus-induced immunogenic cues on oncolytic virotherapy. Sci Rep *14*, 28861. https://doi.org/10.1038/s41598-024-80542-8.

36. Chen, S. (2023). Manipulating immune cells — a therapeutic strategy for cancer and inflammatory disease: https://doi.org/10.33612/diss.822658140.

37. Kurena, B., Müller, E., Christopoulos, P.F., Johnsen, I.B., Stankovic, B., Øynebråten, I., Corthay, A., and Zajakina, A. (2017). Generation and Functional In Vitro Analysis of Semliki Forest Virus Vectors Encoding TNF-α and IFN-γ. Frontiers in Immunology *8*. https://doi.org/10.3389/fimmu.2017.01667.

38. Weigelin, B., den Boer, A.Th., Wagena, E., Broen, K., Dolstra, H., de Boer, R.J., Figdor, C.G., Textor, J., and Friedl, P. (2021). Cytotoxic T-cells are able to efficiently eliminate cancer cells by additive cytotoxicity. Nat Commun *12*, 5217. https://doi.org/10.1038/s41467-021-25282-3.

39. Masemann, D., Köther, K., Kuhlencord, M., Varga, G., Roth, J., Lichty, B.D., Rapp, U.R., Wixler, V., and Ludwig, S. (2018). Oncolytic influenza virus infection restores immunocompetence of lung tumor-associated alveolar macrophages. OncoImmunology *7*, e1423171. https://doi.org/10.1080/2162402X.2017.1423171.

40. Pulaski, B.A., Smyth, M.J., and Ostrand-Rosenberg, S. (2002). Interferon-gamma-dependent phagocytic cells are a critical component of innate immunity against metastatic mammary carcinoma. Cancer Res *62*, 4406–4412.

41. Van Den Bossche, W.B.L., Kleijn, A., Teunissen, C.E., Voerman, J.S.A., Teodosio, C., Noske, D.P., Van Dongen, J.J.M., Dirven, C.M.F., and Lamfers, M.L.M. (2018). Oncolytic virotherapy in glioblastoma patients induces a tumor macrophage phenotypic shift leading to an altered glioblastoma microenvironment. Neuro-Oncology *20*, 1494–1504. https://doi.org/10.1093/neuonc/noy082.

42. Meisen, W.H., Wohleb, E.S., Jaime-Ramirez, A.C., Bolyard, C., Yoo, J.Y., Russell, L., Hardcastle, J., Dubin, S., Muili, K., Yu, J., et al. (2015). The Impact of Macrophage- and Microglia-Secreted TNFα on Oncolytic HSV-1 Therapy in the Glioblastoma Tumor Microenvironment. Clin Cancer Res *21*, 3274–3285. https://doi.org/10.1158/1078-0432.CCR-14-3118.

43. Saha, D., Martuza, R.L., and Rabkin, S.D. (2017). Macrophage Polarization Contributes to Glioblastoma Eradication by Combination Immunovirotherapy and Immune Checkpoint Blockade. Cancer Cell *32*, 253-267.e5. https://doi.org/10.1016/j.ccell.2017.07.006.

44. Fulci, G., Dmitrieva, N., Gianni, D., Fontana, E.J., Pan, X., Lu, Y., Kaufman, C.S., Kaur, B., Lawler, S.E., Lee, R.J., et al. (2007). Depletion of Peripheral Macrophages and Brain Microglia Increases Brain Tumor Titers of Oncolytic Viruses. Cancer Research *67*, 9398–9406. https://doi.org/10.1158/0008-5472.CAN-07-1063.

45. Thoresen, D., Wang, W., Galls, D., Guo, R., Xu, L., and Pyle, A.M. (2021). The molecular mechanism of RIG-I activation and signaling. Immunol Rev *304*, 154–168. https://doi.org/10.1111/imr.13022.

46. Rojas, J.J., Sampath, P., Bonilla, B., Ashley, A., Hou, W., Byrd, D., and Thorne, S.H. (2016). Manipulating TLR Signaling Increases the Anti-tumor T-cell Response Induced by Viral Cancer Therapies. Cell Rep *15*, 264–273. https://doi.org/10.1016/j.celrep.2016.03.017.

47. Muñoz-Rojas, A.R., Kelsey, I., Pappalardo, J.L., Chen, M., and Miller-Jensen, K. (2021). Co-stimulation with opposing macrophage polarization cues leads to orthogonal secretion programs in individual cells. Nat Commun *12*, 301. https://doi.org/10.1038/s41467-020-20540-2.

48. Piccolo, V., Curina, A., Genua, M., Ghisletti, S., Simonatto, M., Sabò, A., Amati, B., Ostuni, R., and Natoli, G. (2017). Opposing macrophage polarization programs show extensive epigenomic and transcriptional cross-talk. Nat Immunol *18*, 530–540. https://doi.org/10.1038/ni.3710.

49. Stout, R.D., Jiang, C., Matta, B., Tietzel, I., Watkins, S.K., and Suttles, J. (2005). Macrophages Sequentially Change Their Functional Phenotype in Response to Changes in Microenvironmental Influences. The Journal of Immunology *175*, 342–349. https://doi.org/10.4049/jimmunol.175.1.342.

50. Lavin, Y., Winter, D., Blecher-Gonen, R., David, E., Keren-Shaul, H., Merad, M., Jung, S., and Amit, I. (2014). Tissue-Resident Macrophage Enhancer Landscapes Are Shaped by the Local Microenvironment. Cell *159*, 1312–1326. https://doi.org/10.1016/j.cell.2014.11.018.

51. Müller, E., Speth, M., Christopoulos, P.F., Lunde, A., Avdagic, A., Øynebråten, I., and Corthay, A. (2018). Both Type I and Type II Interferons Can Activate Antitumor M1 Macrophages When Combined With TLR Stimulation. Front. Immunol. *9*, 2520. https://doi.org/10.3389/fimmu.2018.02520.

52. Meissner, R., Wixler, V., Wulfert, F.P., Jacob, J.C., Hale, B.G., Robeck, T., Masemann, D., Boergeling, Y., and Ludwig, S. (2023). Replication-incompetent influenza A viruses armed with IFN-γ effectively mediate immune modulation and tumor destruction in mice harboring lung cancer. Molecular Therapy - Oncolytics *31*, 100741. https://doi.org/10.1016/j.omto.2023.100741.

53. Bourgeois-Daigneault, M.-C., Roy, D.G., Falls, T., Twumasi-Boateng, K., St-Germain, L.E., Marguerie, M., Garcia, V., Selman, M., Jennings, V.A., Pettigrew, J., et al. (2016). Oncolytic vesicular stomatitis virus expressing interferon-σ has enhanced therapeutic activity. Molecular Therapy - Oncolytics *3*, 16001. https://doi.org/10.1038/mto.2016.1.

54. Singh, A., Koutsoumpli, G., Van De Wall, S., and Daemen, T. (2019). An alphavirus-based therapeutic cancer vaccine: from design to clinical trial. Cancer Immunol Immunother *68*, 849–859. https://doi.org/10.1007/s00262-018-2276-z.

Figure legends

Figure 1: Effect of macrophage frequency on rSFV-mediated tumor infection. (A) Illustration explaining the mode of action of rSFV encoding either GFP or an immunogenic signal used as a non-replicating "suicidal" virotherapy. **(B)** Schematic of the experimental setup for studying rSFV infection in a pancreatic cancer cell line (PANC-1) cocultured with macrophages in both monolayer (2D) and spheroid (3D) spatial organizations. The frequency of macrophages and cancer cells were controlled at the time of initiating the coculture. The coculture setup showing representative images of **(C)** spheroids or **(D)** monolayers composed of cancer cells, infected cells (green, GFP+ cells), and varying frequencies of macrophages (red, stained with FarRed dye) after 24 hours post infection with rSFV encoding GFP (rSFV-GFP). **(E)** Diagram illustrating experimental setups with varying frequencies of macrophages and cancer cells. Top row (variable setup): Frequency of macrophages and cancer cells are varied. Bottom row (constant setup): Frequency of macrophages is varied while cancer cells are kept constant. The grey cells indicate empty space that can be occupied by either cancer cells or macrophages. Quantitative analysis of GFP expression indicating virus infection in the **(F)** spheroid and **(G)** monolayer coculture setups. The plots represent data from 4 replicates of respective coculture methods. Data are presented as mean values±SD.

Figure 2: Effect of macrophage phenotype on rSFV-mediated tumor infection. (A) Schematic of the experimental setup for polarizing peripheral blood derived macrophages to either a naïve (M_{naive}) or or an anti-tumoral ($M_{LPS+IFNγ}$ or M1-like), or a pro-tumoral (M_{IL4} or M2-like) phenotype using cytokines. **(B)** The surface expression of immunomodulatory proteins involved in anti-tumoral (CD80, CD86) and pro-tumoral (CD206, CD163) macrophage activity. **(C)** Principle component analysis of the differences in the phenotypes of macrophages from various healthy blood donors (n=5). Representative images of rSFV infection (green, GFP+ cells) in a pancreatic cancer cell line (PANC-1) cocultured with M_{naive} and M_{IL4} macrophages in both spheroid **(D)** and monolayer **(E)** spatial organizations. Quantitative analysis of GFP expression indicating virus infection in the **(F)** spheroid and **(G)** monolayer coculture of PANC-1 cells with M_{naive} and M_{IL4} macrophages. **(H)** Quantification of GFP expression in monolayer coculture of Ca-Ski cancer cells with M_{naive} and M_{IL4} macrophages. The plots represent data from 4 replicates of respective coculture methods. Data are presented as mean values±SD.

Figure 3: Predicting the outcomes of immunogenic-rSFV therapy using a spatiotemporal model of tumor development. (A) Snapshot of a simulation. Left: Spatial structure of a tumor containing uninfected cancer cells (red), infected cancer cells (green), and macrophages (blue). Right: Distribution of immunogenic signals (magenta) released from dying infected cancer cells, which stimulate a cytotoxic anti-cancer T-cell response. **(B)** Time trajectory illustrating the dynamics of a suicidal rSFV-therapy. Initially, uninfected cancer cells are targeted by the virus and weakly attacked by T-cells. Over time, virus-killed cancer cells release immunogenic signals, boosting T-cell cytotoxicity. Finally, the boosting effect wanes as immunogenic signal-levels diminish. **(C)** Effect of the amount of immunogenic signal produced per infected cells on the probability of tumor eradication. The colors indicate five simulation scenarios differing in the percentage of infected cells at the time of infection. **(D)** The effect of anticancer T-cell cytotoxicity rates on the probability of tumor eradication. **(E)** The effect of macrophage frequency at the time of rSFV therapy on the probability of tumor eradication. When not specifically under consideration, the parameter values were kept at their default values: the amount of immunogenic signal released was set to 0.25, the T-cell cytotoxicity rate was set to 5, and the number of macrophages was set to 2500. Colored dotted lines indicate the mean values, colored envelopes indicate the 95% confidence interval obtained via bootstrapping. Each panel represents 10000 simulations for respective parameter combinations.

Figure 4: Impact of IFN-γ on tumor associated macrophage and T-cells in the tumor microenvironment. (A) Schematic of cytokine production and reception by T-cells and macrophages (MØ), highlighting IFN-γ, IL-10, and IL-4 as key cytokines involved in influencing both cell types. Cytokine interactions are color-coded based on their impact on tumor progression: pro-tumoral (purple) and antitumoral (orange). **(B)** The effective concentration range of various cytokines (EC_{50}) with the points indicating the maximum and minimum experimentally reported limits (as per [32]). **(C)** Analysis process of cervical (CESC, 300 samples) and pancreatic (PAAD, 151 samples) cancer patient datasets stored at The Cancer Genome Atlas (TCGA) by using the CRI iAtlas online platform to correlate the presence of macrophage types with T-cells and IFN-γ signature. **(D)** Correlation heatmap of intra-tumoral IFN-γ signature with presence of various macrophage phenotypes. **(E-H)** Scatter plots showing the relationship between the intra-tumoral IFN-γ signature with the presence of classical (M_{class} or M1-like) and alternatively activated (M_{alter} or M2-like) macrophages in cervical or pancreatic cancer patients. **(I)** Correlation heatmap of intra-tumoral fraction of cytotoxic (CD8) T-cells with presence of various macrophage phenotypes. **(J-M)** Scatter plots showing the relationship between the intra-tumoral fraction of CD8 T-cells with the presence of M_{class} or M_{alter} macrophages in cervical or pancreatic cancer patients.

Figure 5: Evaluation of T-cell activation in tumor-immune monolayer cocultures by rSFV. (A) Schematic representation of the experimental setup consisting of tumor-immune monolayer cocultures of cancer cells and macrophages treated with rSFV, followed by the addition of PBMCs to introduce T-cells and evaluate their activation. Flow cytometry analysis to measure activation of **(B)** CD4 helper T-cells and **(C)** CD8 cytotoxic T-cells based on the expression of CD69 and CD107a proteins, marked in the upper right quadrant in each panel. rSFV-GFP treated cocultures are indicated in green and rSFV-IFN-γ treated cocultures in red. The representative plots in (B-C) illustrate T-cell activation in the context of PANC-1 cancer cells in coculture with either M_{naive} or M_{IL4} macrophages in different frequencies. Quantification of **(D)** CD4 helper T-cell or **(E)** CD8 cytotoxic T-cell activation in the tumor-immune cocultures by rSFV. The plots represent data from 4 replicates. Data are presented as mean values ± SD.

Figure 6: Evaluation of T-cell activation in tumor-immune spheroid co-cultures upon rSFV infection. (A) Schematic representation of the experimental setup consisting of tumor-immune spheroid cocultures of cancer cells and macrophages treated with rSFV, followed by the addition of PBMCs to introduce T-cells and evaluate their activation. Flow cytometry analysis to measure activation of T-cells as explained in Figure 6. Quantification of **(B)** CD4 helper T-cell or **(C)** CD8 cytotoxic T-cell activation in the tumor-immune cocultures by rSFV. rSFV-GFP treated cocultures are indicated in green and rSFV-IFN-γ treated cocultures in red. The plots represent data from 4 replicates. Data are presented as mean values ± SD.

Figure 7: Influence of rSFV infection on macrophage phenotype. (A) Experimental setup to study changes in macrophage phenotype upon stimulation by rSFV. This includes studying the effect of **(B)** either rSFV-particles alone, **(C)** or by infected cells alone, **(D)** or by both. **(E)** Heatmap of change in cell-surface expression of proteins involved in either pro-tumoral (CD206) or anti-tumoral (CD80, CD86) function of M_{IL4} macrophages cocultured or not with PANC-1 cancer cells upon stimulation resulting from rSFV particles and/or infected cells. Heatmap of M_{naive} and M_{IL4} macrophage cell-surface protein expression upon stimulation with **(F)** rSFV particles alone, or both virus particles and infected **(G-H)** PANC-1 or **(I-J)** Ca-Ski cancer cells. The plots represent mean value data from 4 replicates.

Figure 1

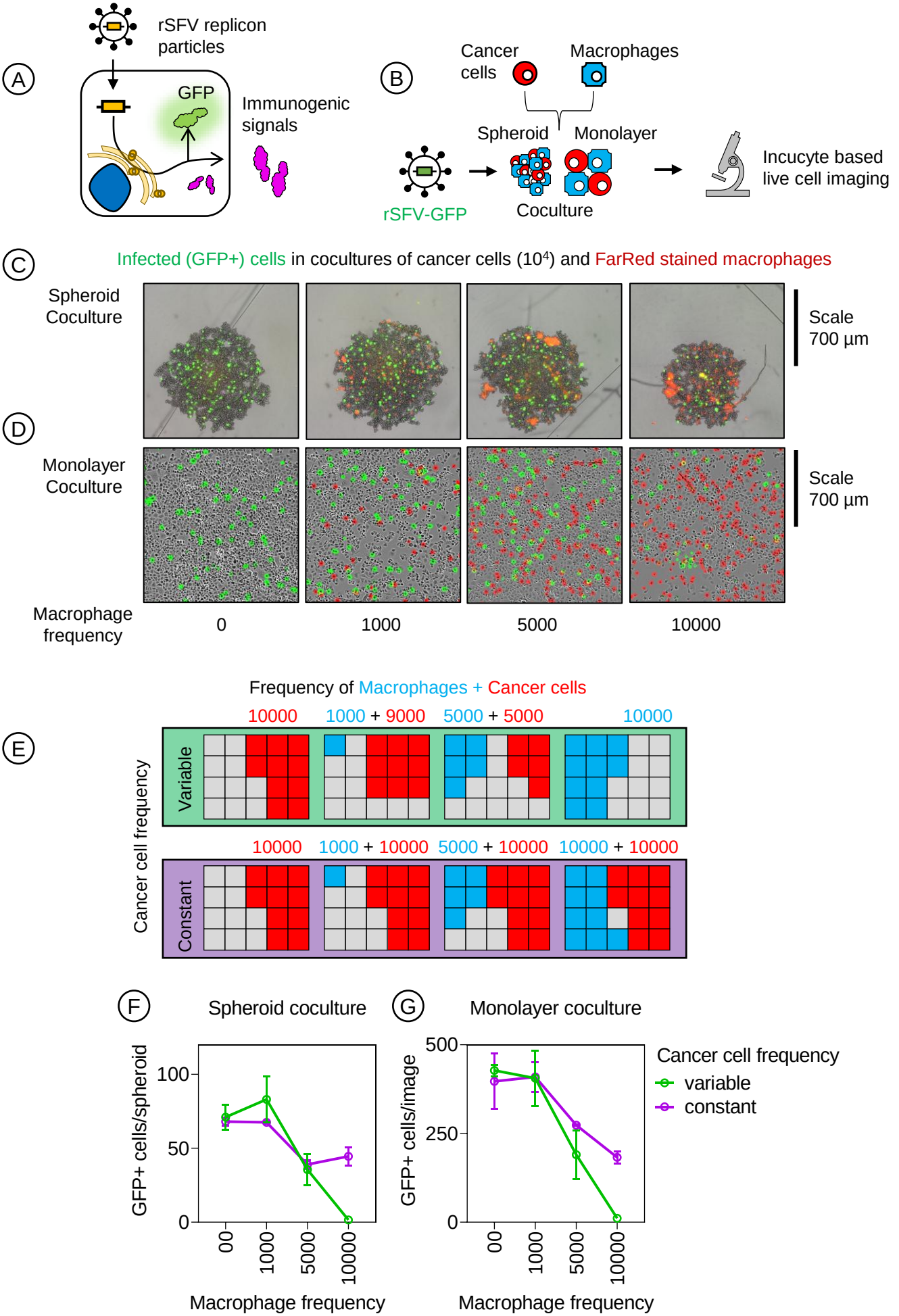
A
rSFV replicon particles
GFP
Immunogenic signals
B
Cancer cells
Macrophages
Spheroid
Monolayer
rSFV-GFP
Coculture
Incucyte based live cell imaging
C
Infected (GFP+) cells in cocultures of cancer cells (10⁴) and FarRed stained macrophages
Spheroid Coculture
Scale 700 µm
D
Monolayer Coculture
Scale 700 µm
Macrophage frequency
0
1000
5000
10000
E
Frequency of Macrophages + Cancer cells
10000
1000 + 9000
5000 + 5000
10000
Cancer cell frequency
Variable
10000
1000 + 10000
5000 + 10000
10000 + 10000
Constant
F
Spheroid coculture
GFP+ cells/spheroid
100
50
0
00
1000
5000
10000
Macrophage frequency
G
Monolayer coculture
GFP+ cells/image
500
250
0
00
1000
5000
10000
Macrophage frequency
Cancer cell frequency
variable
constant

Figure 2

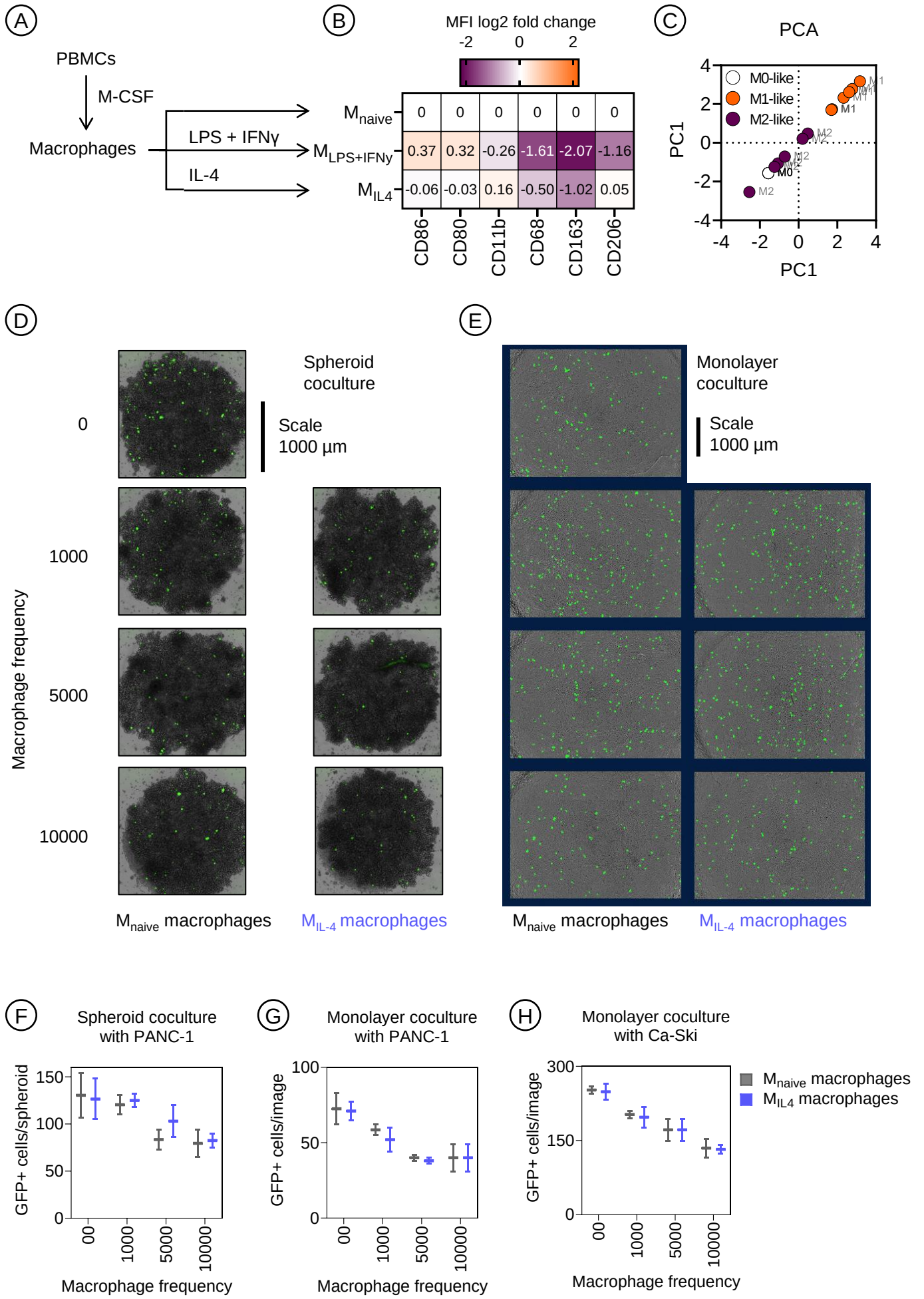
A
PBMCs
M-CSF
Macrophages
LPS + IFNγ
IL-4
B
MFI log2 fold change
-2
0
2
M naive
M LPS+IFNγ
M IL4
0 0 0 0 0 0
0.37 0.32 -0.26 -1.61 -2.07 -1.16
-0.06 -0.03 0.16 -0.50 -1.02 0.05
CD86
CD80
CD11b
CD68
CD163
CD206
C
PCA
M0-like
M1-like
M2-like
PC1
PC1
D
Spheroid coculture
Scale 1000 µm
Macrophage frequency
0
1000
5000
10000
M naive macrophages
M IL-4 macrophages
E
Monolayer coculture
Scale 1000 µm
M naive macrophages
M IL-4 macrophages
F
Spheroid coculture with PANC-1
GFP+ cells/spheroid
Macrophage frequency
G
Monolayer coculture with PANC-1
GFP+ cells/image
Macrophage frequency
H
Monolayer coculture with Ca-Ski
GFP+ cells/image
Macrophage frequency
M naive macrophages
M IL4 macrophages

Figure 3

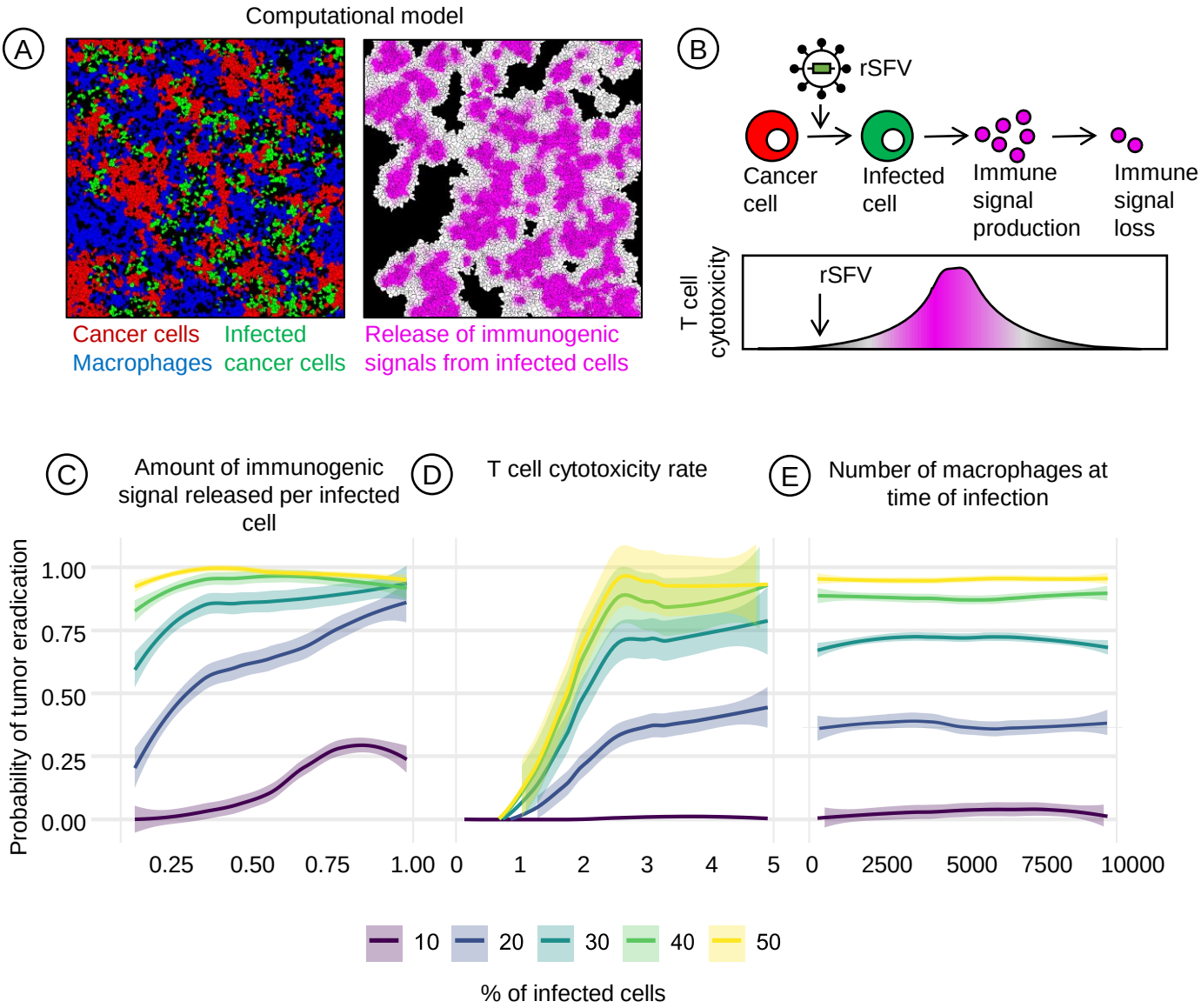
A
Computational model
Cancer cells
Infected cancer cells
Macrophages
Release of immunogenic signals from infected cells
B
rSFV
Cancer cell
Infected cell
Immune signal production
Immune signal loss
T cell cytotoxicity
rSFV
C
Amount of immunogenic signal released per infected cell
D
T cell cytotoxicity rate
E
Number of macrophages at time of infection
Probability of tumor eradication
1.00
0.75
0.50
0.25
0.00
0.25
0.50
0.75
1.00
0
1
2
3
4
5
0
2500
5000
7500
10000
10
20
30
40
50
% of infected cells

Figure 4

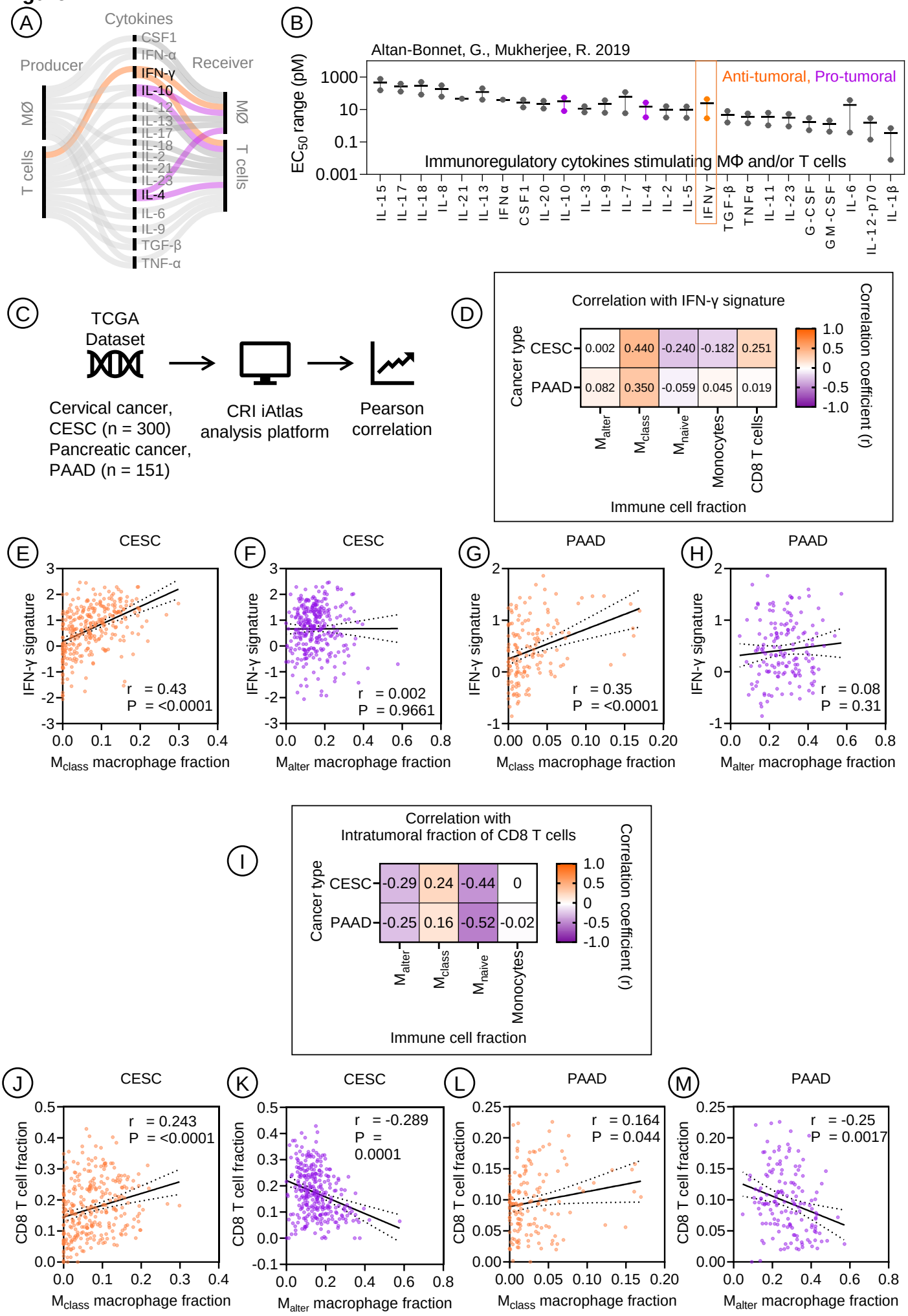
A
Cytokines
Producer
Receiver
MØ
T cells
CSF1
IFN-α
IFN-γ
IL-10
IL-12
IL-13
IL-17
IL-18
IL-2
IL-21
IL-23
IL-4
IL-6
IL-9
TGF-β
TNF-α
B
Altan-Bonnet, G., Mukherjee, R. 2019
EC50 range (pM)
Anti-tumoral, Pro-tumoral
Immunoregulatory cytokines stimulating MΦ and/or T cells
C
TCGA Dataset
Cervical cancer, CESC (n = 300)
Pancreatic cancer, PAAD (n = 151)
CRI iAtlas analysis platform
Pearson correlation
D
Correlation with IFN-γ signature
Cancer type
CESC 0.002 0.440 -0.240 -0.182 0.251
PAAD 0.082 0.350 -0.059 0.045 0.019
Malter Mclass Mnaive Monocytes CD8 T cells
Immune cell fraction
Correlation coefficient (r)
E CESC r = 0.43 P = <0.0001
F CESC r = 0.002 P = 0.9661
G PAAD r = 0.35 P = <0.0001
H PAAD r = 0.08 P = 0.31
IFN-γ signature
Mclass macrophage fraction
Malter macrophage fraction
I
Correlation with Intratumoral fraction of CD8 T cells
Cancer type
CESC -0.29 0.24 -0.44 0
PAAD -0.25 0.16 -0.52 -0.02
Malter Mclass Mnaive Monocytes
Immune cell fraction
Correlation coefficient (r)
J CESC r = 0.243 P = <0.0001
K CESC r = -0.289 P = 0.0001
L PAAD r = 0.164 P = 0.044
M PAAD r = -0.25 P = 0.0017
CD8 T cell fraction
Mclass macrophage fraction
Malter macrophage fraction

Figure 5

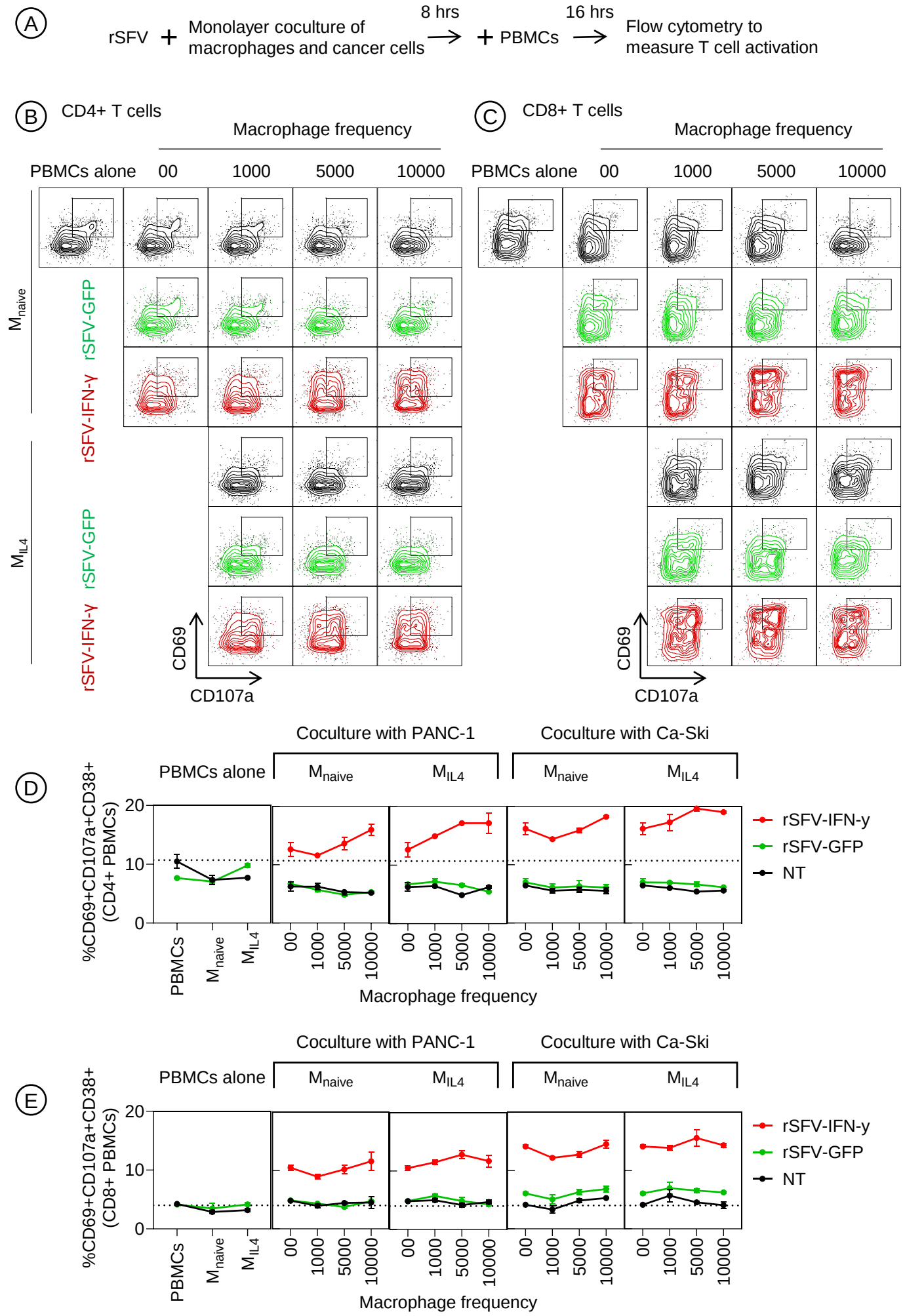
A
rSFV + Monolayer coculture of macrophages and cancer cells
8 hrs
+ PBMCs
16 hrs
Flow cytometry to measure T cell activation
B
CD4+ T cells
Macrophage frequency
PBMCs alone
00
1000
5000
10000
M naive
M IL4
rSFV-GFP
rSFV-IFN-γ
CD69
CD107a
C
CD8+ T cells
Macrophage frequency
PBMCs alone
00
1000
5000
10000
CD69
CD107a
D
Coculture with PANC-1
Coculture with Ca-Ski
PBMCs alone
M naive
M IL4
%CD69+CD107a+CD38+ (CD4+ PBMCs)
20
10
0
PBMCs
00
1000
5000
10000
Macrophage frequency
rSFV-IFN-y
rSFV-GFP
NT
E
Coculture with PANC-1
Coculture with Ca-Ski
PBMCs alone
M naive
M IL4
%CD69+CD107a+CD38+ (CD8+ PBMCs)
20
10
0
PBMCs
00
1000
5000
10000
Macrophage frequency
rSFV-IFN-y
rSFV-GFP
NT

Figure 6

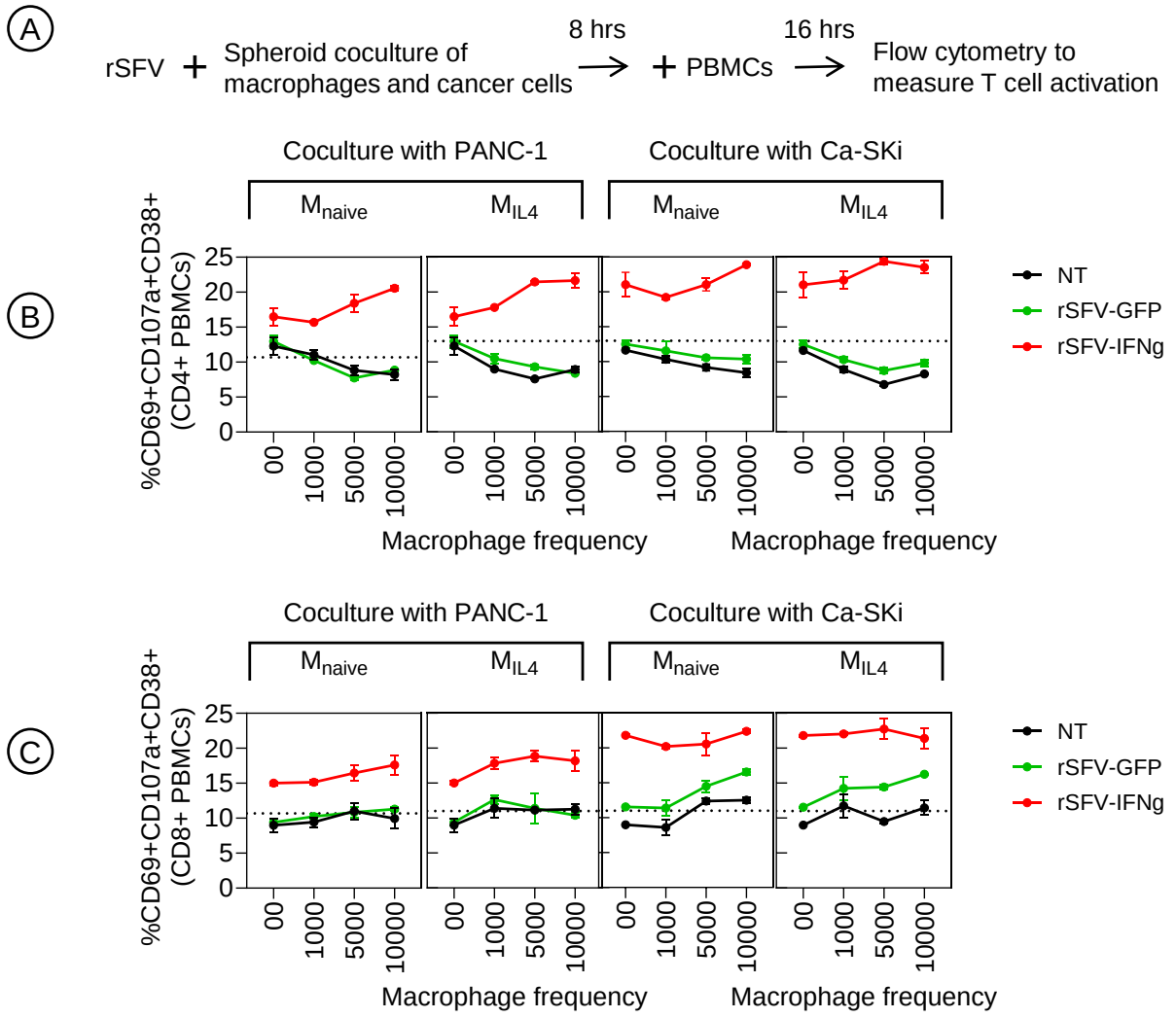
A
rSFV + Spheroid coculture of macrophages and cancer cells
8 hrs
+ PBMCs
16 hrs
Flow cytometry to measure T cell activation
B
Coculture with PANC-1
Coculture with Ca-SKi
M naive
M IL4
%CD69+CD107a+CD38+ (CD4+ PBMCs)
Macrophage frequency
NT
rSFV-GFP
rSFV-IFNg
C
%CD69+CD107a+CD38+ (CD8+ PBMCs)

Figure 7

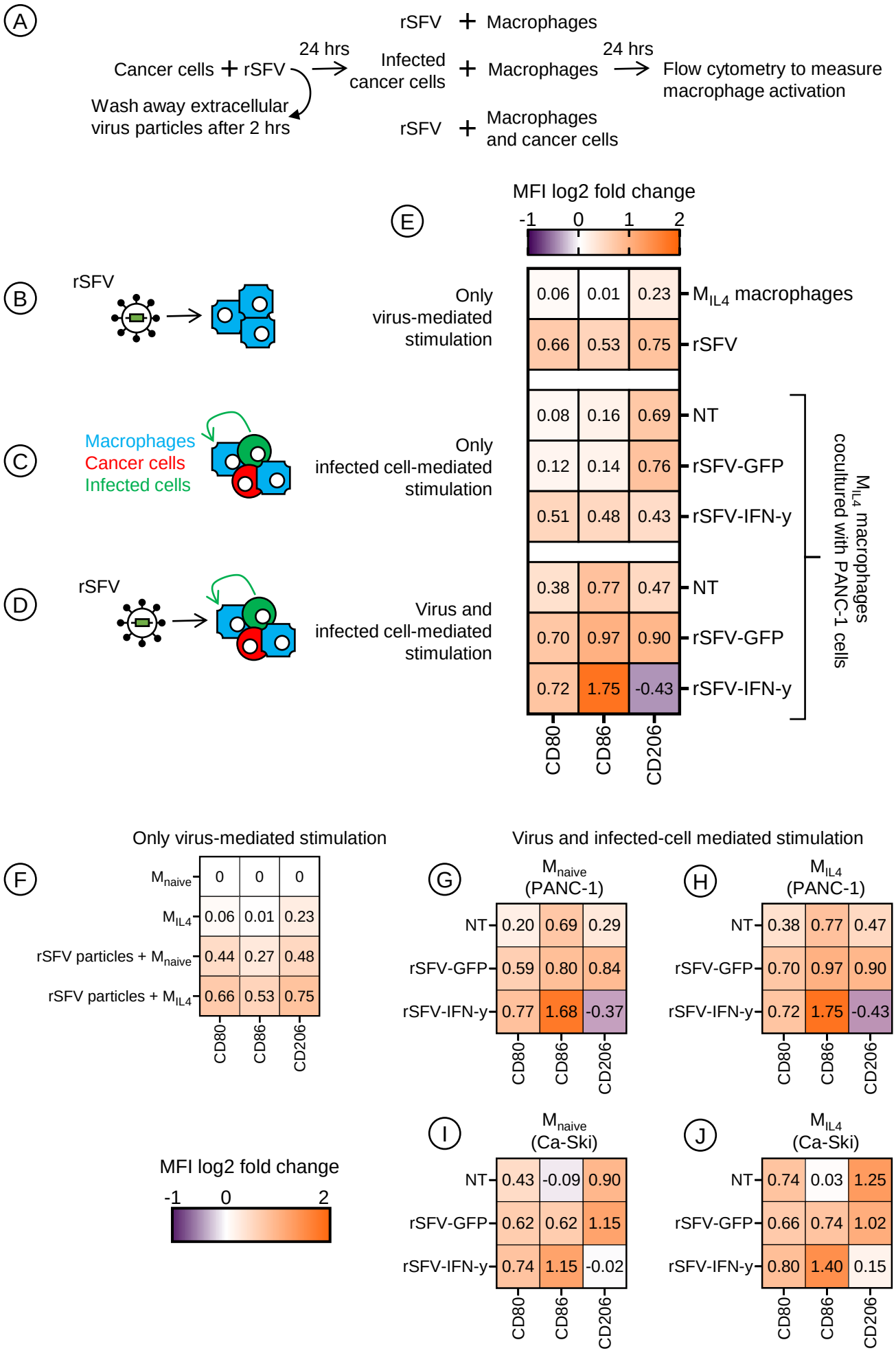
A
Cancer cells + rSFV
24 hrs
Wash away extracellular virus particles after 2 hrs
rSFV + Macrophages
Infected cancer cells + Macrophages
rSFV + Macrophages and cancer cells
24 hrs
Flow cytometry to measure macrophage activation
B
rSFV
C
Macrophages
Cancer cells
Infected cells
D
rSFV
E
MFI log2 fold change
-1 0 1 2
Only virus-mediated stimulation
Only infected cell-mediated stimulation
Virus and infected cell-mediated stimulation
M_IL4 macrophages
rSFV
NT
rSFV-GFP
rSFV-IFN-y
NT
rSFV-GFP
rSFV-IFN-y
M_IL4 macrophages cocultured with PANC-1 cells
CD80 CD86 CD206
0.06 0.01 0.23
0.66 0.53 0.75
0.08 0.16 0.69
0.12 0.14 0.76
0.51 0.48 0.43
0.38 0.77 0.47
0.70 0.97 0.90
0.72 1.75 -0.43
F
Only virus-mediated stimulation
M_naive 0 0 0
M_IL4 0.06 0.01 0.23
rSFV particles + M_naive 0.44 0.27 0.48
rSFV particles + M_IL4 0.66 0.53 0.75
CD80 CD86 CD206
Virus and infected-cell mediated stimulation
G
M_naive (PANC-1)
NT 0.20 0.69 0.29
rSFV-GFP 0.59 0.80 0.84
rSFV-IFN-y 0.77 1.68 -0.37
H
M_IL4 (PANC-1)
NT 0.38 0.77 0.47
rSFV-GFP 0.70 0.97 0.90
rSFV-IFN-y 0.72 1.75 -0.43
I
M_naive (Ca-Ski)
NT 0.43 -0.09 0.90
rSFV-GFP 0.62 0.62 1.15
rSFV-IFN-y 0.74 1.15 -0.02
J
M_IL4 (Ca-Ski)
NT 0.74 0.03 1.25
rSFV-GFP 0.66 0.74 1.02
rSFV-IFN-y 0.80 1.40 0.15
MFI log2 fold change
-1 0 2